Fault lubrication during earthquakes

Article *in* Nature · March 2011

DOI: 10.1038/nature09838

CITATIONS
819

READS
1,585

9 authors, including:

Giulio Di Toro
University of Padova
240 PUBLICATIONS **8,160** CITATIONS
SEE PROFILE

Takehiro Hirose
Japan Agency for Marine-Earth Science Technology
172 PUBLICATIONS **6,499** CITATIONS
SEE PROFILE

Stefan Nielsen
Durham University
166 PUBLICATIONS **6,518** CITATIONS
SEE PROFILE

Kazuo Mizoguchi
Central Research Institute of Electric Power Industry
71 PUBLICATIONS **2,256** CITATIONS
SEE PROFILE

LETTER

doi:10.1038/nature09838

Fault lubrication during earthquakes

G. Di Toro[1,2], R. Han[3], T. Hirose[4], N. De Paola[5], S. Nielsen[2], K. Mizoguchi[6], F. Ferri[1], M. Cocco[2] & T. Shimamoto[7]

The determination of rock friction at seismic slip rates (about 1 m s^{-1}) is of paramount importance in earthquake mechanics, as fault friction controls the stress drop, the mechanical work and the frictional heat generated during slip[1]. Given the difficulty in determining friction by seismological methods[1], elucidating constraints are derived from experimental studies[2–9]. Here we review a large set of published and unpublished experiments (~300) performed in rotary shear apparatus at slip rates of 0.1–2.6 m s^{-1}. The experiments indicate a significant decrease in friction (of up to one order of magnitude), which we term fault lubrication, both for cohesive (silicate-built[4–6], quartz-built[3] and carbonate-built[7,8]) rocks and non-cohesive rocks (clay-rich[9], anhydrite, gypsum and dolomite[10] gouges) typical of crustal seismogenic sources. The available mechanical work and the associated temperature rise in the slipping zone trigger[11,12] a number of physicochemical processes (gelification, decarbonation and dehydration reactions, melting and so on) whose products are responsible for fault lubrication. The similarity between (1) experimental and natural fault products and (2) mechanical work measures resulting from these laboratory experiments and seismological estimates[13,14] suggests that it is reasonable to extrapolate experimental data to conditions typical of earthquake nucleation depths (7–15 km). It seems that faults are lubricated during earthquakes, irrespective of the fault rock composition and of the specific weakening mechanism involved.

The evolution of friction (shear stress, τ) during earthquakes and the dynamic friction coefficient, μ, are key parameters in controlling seismic fault slip and radiated energy[1,13]. In the past 40 years, experiments performed in triaxial and biaxial apparatuses under conditions of low slip rates ($V < 1$ mm s^{-1}) and modest displacements ($\delta < 1$ cm) have shown that the friction coefficient in cohesive and non-cohesive rocks is about 0.7 (ref. 15) irrespective of the rock type (with a few exceptions that are of great relevance for the mechanics of mature faults), and that frictional instabilities of a few per cent[16–19], described by rate-and-state friction laws[19], are associated with earthquake initiation. Although the above results are consistent with several seismological and geophysical observations[17,18], the experiments were performed at slip rates and displacements orders of magnitude smaller than those typical of earthquakes[20] (0.1–10 m s^{-1} and up to 20 m, respectively). Given the low slip rates, these experiments lack a primary aspect of natural seismic slip: a large mechanical work rate (or instantaneous power density, $\Phi(t) = \tau(t)V(t)$) within the slipping zone[14]. The work rate can be so large as to grind and mill the rock (producing particles of nanometric size, or nanopowders), trigger mechanically and thermally activated[21] chemical reactions, and, eventually, melt the rock[22]. Under these extreme deformation conditions, the fault surfaces are separated by fluids or other tribochemical products (for example melt, gel, nanopowders and decarbonation products). Work rate (not work alone) is the key parameter, as a given amount of work exchanged at a slow rate is buffered by dissipative processes and hence produces limited reactions.

In the past 15 years, the installation and exploitation of rotary shear apparatus[2,3,5] designed to achieve the larger slip rates and displacements typical of earthquakes produced unexpected experimental results. Among these, the most surprising is the dramatic drop in friction (of up to 90% in most cases) at seismic slip rates, independent of the rock type and the weakening mechanism used.

Here we report about 300 published and unpublished high-velocity rock friction experiments performed in the rotary shear apparatuses at Brown University[3] and at Kyoto University[5] (now at the Kochi Institute for Core Sample Research, JAMSTEC). These experiments were performed at room humidity with 0.1 m s^{-1} $< V <$ 2.6 m s^{-1}, $\delta > 2$ m and 0.6 MPa $< \sigma_n <$ 20 MPa (normal stress) on solid cylinders (22 and 40 mm in diameter) or hollow cylinders (15/25, 15/39, 27/39 and 40/50 mm in internal/external diameter) in the case of cohesive rock and on gouge layers confined by Teflon rings[9] in the case of non-cohesive rock. Figure 1 summarizes the friction coefficient as a function of normalized displacement in experiments performed at seismic slip rates for cohesive and non-cohesive rocks: both show a similar exponential decay of friction from a peak (P) to a steady-state value (SS). In all the experiments, friction decreases significantly with increasing slip. Here we introduce the thermal slip distance, D_{th}, defined as the slip distance over which the friction coefficient decays to a value $\mu_{th} = \mu_{ss} + (\mu_p - \mu_{ss})/e$ (the experimental data are fitted by an exponential decay from a peak value, μ_p, to a steady-state value, μ_{ss}).

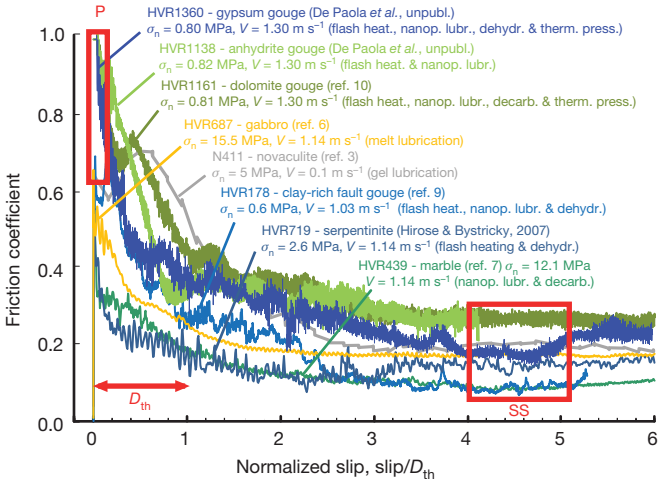

Figure 1 | Friction coefficient versus normalized slip. Shear stress and slip were normalized with respect to normal stress and the thermal slip distance, D_{th}, respectively. The displacement was normalized because experiments performed with different rocks and under different normal stresses had different D_{th} values (Supplementary Information, section 4, and Fig. 2). The friction coefficient decays exponentially with slip from a peak (P) at the initiation of sliding to a steady-state (SS) value. The weakening mechanisms that we assume to be dominant are shown in parentheses (flash heat., flash heating; nanop. lubr., nanopowder lubrication; dehydr., dehydration reaction; decarb., decarbonation reaction; therm. press., thermal pressure). For all the weakening mechanisms, the friction coefficient in the steady state is <0.3. Unpubl., unpublished experimental data. See Supplementary Information, section 2, for the reference to Hirose and Bystricky, 2007.

[1]Dipartimento di Geoscienze, Università di Padova, Padova 35131, Italy. [2]Istituto Nazionale di Geofisica e Vulcanologia, Roma 00143, Italy. [3]Korea Institute of Geoscience and Mineral Resources, Daejeon 305-350, South Korea. [4]Kochi Institute for Core Sample Research, JAMSTEC, Kochi 783-8502, Japan. [5]Department of Earth Sciences, University of Durham, Durham DH1 3LE, UK. [6]Civil Engineering Research Laboratory, Central Research Institute of Electric Power Industry, Chiba 270-1194, Japan. [7]Institute of Geology, China Earthquake Administration, Beijing 100029, China.

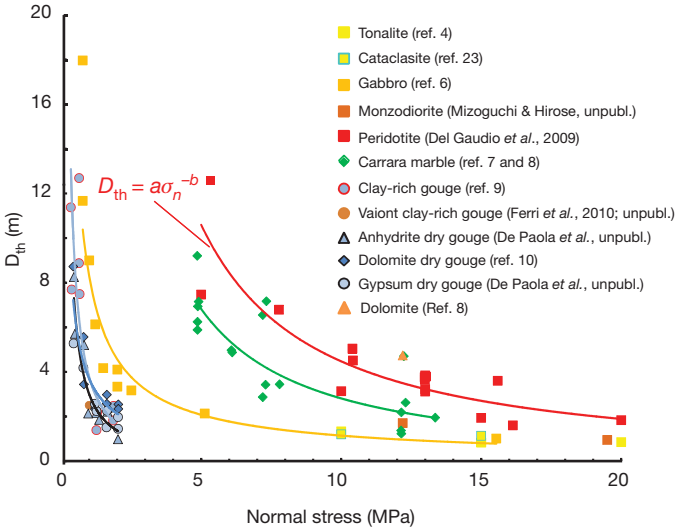

Figure 2 | The thermal slip distance, D_{th}, versus normal stress from experiments performed with $V = 1$–$1.6\ m\ s^{-1}$. This plot shows that different rocks (and weakening mechanisms) have different D_{th} values and that D_{th} decreases with increasing σ_n (power-law dependence with a general form $D_{th} = a\sigma_n^{-b}$, where a and b are experimentally determined coefficients). For peridotite, $a = 78$ and $b = 1.24$; for anhydrite, $a = 3$ and $b = 1.13$. By extrapolating the best-fit curves to seismogenic depths ($\sigma_n > 200$ MPa), we predict that $D_{th} \approx 7$ cm and ~0.5 cm for peridotite and anhydrite, respectively. It follows that low values of friction are easily achieved during earthquakes in nature. See Supplementary Information, section 2, for references to Del Gaudio *et al.*, 2009, and Ferri *et al.*, 2010.

The thermal slip distance varies significantly between experiments performed on different rocks under the same experimental conditions (mainly the normal stress and the slip rate; Supplementary Information, section 4), but for a given rock type D_{th} seems to decrease according to a power law for increasing normal stress (Fig. 2). For instance, in the case of peridotite, D_{th} decreased from 13 m for $\sigma_n = 5$ MPa to 1.3 m for $\sigma_n = 20$ MPa. The extrapolation of these data to seismogenic depths (>7 km), where normal stresses acting on the fault can be >200 MPa, suggests that D_{th} should decrease to less than 10 cm. Recent theoretical work[6] and field evidence[23] suggest also that D_{th} can decrease to a few centimetres in the presence of melts.

In Fig. 3, we summarize about 300 high-velocity ($V > 0.1\ m\ s^{-1}$) experiments performed on cohesive (for example novaculite, marble, serpentinite, gabbro and tonalite) and non-cohesive rocks (anhydrite, gypsum, dolomite and clay-rich gouges) typical of crustal seismogenic sources (for data, see Supplementary Information, section 2). For each rock type there is a drastic decrease in friction that we interpret as the result of mechanically and thermally activated (that is, tribochemical), often coexisting, weakening mechanisms (see Supplementary Information, section 3, for a summary of the weakening mechanisms). For instance, in calcite-built rocks such as marbles, a significant weakening (to $\mu = 0.03$) was concurrent with the emission of CO_2 from the slipping zone and the production of lime and portlandite nanopowders[7,8]. The maximum measured average temperature was about 900 °C, which is consistent with the thermally activated breakdown temperature for $CaCO_3 \rightarrow CaO + CO_2$. The measured weakening has been attributed[7,8] to thermal decomposition and the production of nanopowders. For melt lubrication, we considered only experiments performed at $\sigma_n > 5$ MPa because the nonlinear dependence of shear stress on normal stress in this case results in an overestimate of the friction coefficient at low normal stresses[6]. The most striking features of Fig. 3 are the velocity dependence of friction at high slip rates, the low steady-state friction at seismic slip rates and the tendency of friction to cluster around a coefficient of about 0.2–0.4 for $V = 1\ m\ s^{-1}$, independently of the invoked weakening mechanism.

Figure 3 does not provide information on the mechanical work rate generated in the slipping zone, which we argue is a key parameter in controlling the rate of temperature increase ($dT/dt \propto \Phi(t)$: if a large amount of work is generated locally within a short time then diffusive heat loss is confined to a small rock volume, resulting in a large temperature rise in the slipping zone[14]) and the onset of mechanically and thermally activated weakening processes. For simplicity, we introduce an equivalent shear stress, $\tau_e = \text{const.}$, to determine the equivalent power density, $\Phi_e \approx \tau_e V$. This constant stress is a thermally balanced average of the variable stress, $\tau(t)$, over a time interval $t_{th} = D_{th}/V$. It is defined such that both τ_e and $\tau(t)$ yield the same temperature increase on the fault over a time t_{th}. If we assume that heat diffuses from an infinitesimally thin shear zone and use an exponential stress decay (Fig. 1), we obtain (Methods)

$$\tau_e = \tau_{ss} + \frac{\sqrt{\pi}\,\mathrm{Erfi}(1)}{2e}(\tau_p - \tau_{ss})$$

Here Erfi is the imaginary error function (Erfi(1) = 1.65043).

The approximation of an infinitesimally thin layer is based on observations of both natural and experimental seismic faults, which show that the shear band active at high slip rates generally decreases in

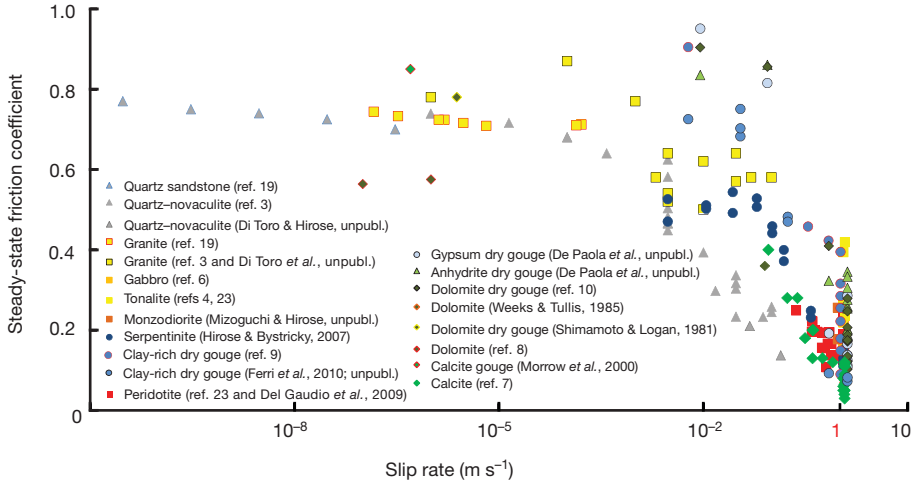

Figure 3 | Steady-state friction coefficient versus slip rate. There is a marked decrease in the friction coefficient when seismic slip rates (~1 m s^{-1}) are approached. Note that slip rate is plotted on a logarithmic scale here. For melt lubrication, we report only experiments performed with $\sigma_n > 5$ MPa (see text). Data and extra references (Hirose and Bystricky, 2007, Ferri *et al.*, 2010, Del Gaudio *et al.*, 2009, Weeks and Tullis, 1985, Shimamoto and Logan, 1981, and Morrow *et al.*, 2000) are in Supplementary Information, section 2.

thickness to a fraction of a millimetre, even for initially thicker gouge layers[7–9,21]. In Fig. 4, we plot the friction coefficient as a function of the power density for cohesive (Fig. 4b) and non-cohesive (Fig. 4c) rocks (for data, see Supplementary Information, section 5). Friction data still show an evident drop approaching the power densities expected in nature (Fig. 4a, grey area), but their scaling with power density depends on the rock type. In particular, weakening of novaculite occurs at lower power densities than does weakening of calcite- and silicate-built rocks. Figure 4a suggests the activation of different dynamic weakening mechanisms associated with different work rates and temperature increases, ΔT, in the slipping zone. Assuming an exponential decay, ΔT can be estimated (Supplementary Information,

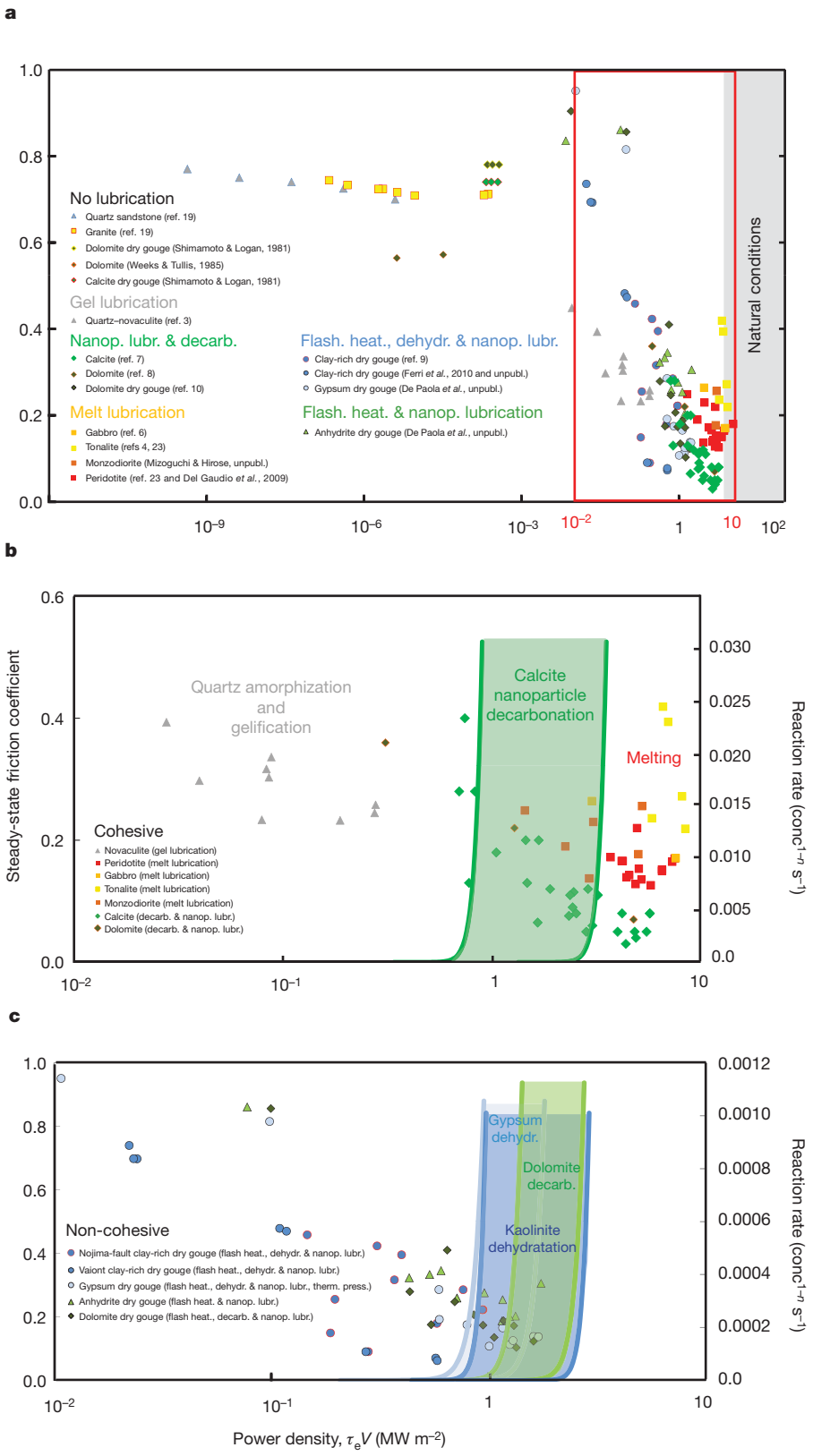

Figure 4 | Steady-state friction coefficient versus power density. **a**, The different weakening mechanisms are activated at increasing power densities, $\tau_e V$ (here plotted on a logarithmic scale), which also reflect the different temperatures (equation (1)) achieved in the slipping zone. The box in red is the inset shown in **b** and **c**. The grey area is for power densities expected in nature. **b**, **c**, Red-boxed region of **a** for cohesive rocks (**b**) and non-cohesive rocks (**c**), showing curves of reaction speed constant, k (right-hand axis, where 'conc' denotes concentration, for example mol dm^{-3}, and n is the order of the reaction), versus power density. Because k varies with $\sqrt{D_{th}/V}$ for a given power density, $\tau_e V$ (equation (2)), for each rock type we plotted curves of reaction speed constant for the highest and lowest values of $\sqrt{D_{th}/V}$ (Methods). In **b**, for cohesive rocks, novaculite weakening at low power densities is indicative of mechanically activated chemical reactions (amorphization and gelification of quartz[2]). Marble weakening is triggered at higher power densities, where thermally activated decarbonation reactions (green curves; we used E_A for decarbonation of calcite nanoparticles; see Supplementary Information, section 5) are more effective. The increase in the reaction rate constant with power density (and temperature) implies the presence of more reaction products in the slipping zone, concomitant with the boost of the weakening mechanism. In **c**, for non-cohesive rocks, dehydration and decarbonation reactions are expected to occur at higher power densities (and temperatures) than those estimated in the slipping zone, suggesting that weakening during the transient stage is dominated by mechanically activated and local, thermally activated reactions and lubrication mechanisms (nanopowder lubrication and flash weakening). Data are in Supplementary Information, section 4, and extra references (Shimamoto and Logan, 1981, Weeks and Tullis, 1985, Del Gaudio *et al.*, 2009, and Ferri *et al.*, 2010) are in Supplementary Information, section 2.

section 4) once a significant friction drop has been triggered (that is, over a slip distance D_{th}):

$$\Delta T(t_{th}=D_{th}/V)=\frac{\tau_e V}{\rho c_p}\sqrt{\frac{D_{th}}{\pi\kappa V}} \quad (1)$$

Here ρ is the rock density, c_p is the specific heat at constant pressure and κ is the thermal diffusivity. Chemical reactions start once an energy barrier (the activation energy, E_A) is overcome. The work rate, $\tau_e V$, and the temperature increase initiate tribochemical reactions governing dynamic fault weakening. Tribochemical reactions include mechanically and thermally activated, short-lived (10^{-3}–10^{-6} s), local (<1 μm) processes operating during rubbing of the sliding surfaces[11,12,24–27], which result in small quantities of reaction products. Rubbing induces plastic deformation, fracturing and amorphization (mechanically activated reactions) and exposes clean, highly reactive and catalytic surfaces (which lower the E_A value of the reaction), as well as flash heating (a local and short-lived, thermally activated reaction) of the asperity contacts[11,12] (which increases the reaction rate). The E_A values of mechanically activated reactions are lower than the E_A values of for thermally activated reactions, and when the reaction is simultaneous with milling, the reaction rate is nearly independent of the bulk temperature[12–24–26] (Supplementary Information, section 5). Eventually, the bulk temperature of the slipping zone increases, direct thermal activation is more effective than mechanical excitation[12] and larger quantities of reaction products are produced. At this stage, the reaction rate is proportional to the reaction speed constant, k (Arrhenius-type dependence on temperature[12]):

$$k=A\exp\left(\frac{-E_A}{R(T_{amb}+\Delta T)}\right)=A\exp\left[\frac{-E_A}{R(T_{amb}+(\tau_e V/\rho c_p)\sqrt{D_{th}/V\pi\kappa})}\right] \quad (2)$$

Here A is the pre-exponential factor, R is the gas constant and T_{amb} is room temperature.

The plot in Fig. 4b, for cohesive rocks, distinguishes weakening resulting from mechanically and local thermally activated reactions (amorphization and gelification of quartz[2]) from that resulting from reactions dominated by thermal activation (decarbonation of calcite[7]). For a power density of 2 MW m^{-2}, which corresponds to an estimated temperature increase of about 800–1,000 °C (see equation (1); Supplementary Information, section 4), in the range of measured temperatures[7], we observe the limit between decarbonation and melting.

For experiments performed on non-cohesive rocks, large weakening occurs before the thermally activated, Arrhenius-type reaction (equation (2)) should dominate, suggesting the operation of other lubricating mechanisms (such as flash weakening at the asperity contacts[14,28] and nanopowder lubrication[8,29]) controlled by mechanically activated and local, thermally activated reactions[11,12,24,25,27].

In summary, high-velocity experiments indicate that at seismic slip rates the friction coefficient decreases to about 10–30% of its initial value (Figs 1 and 3). The extremely low friction data reported in Fig. 3 can occur in nature, implying large breakdown stress decreases (defined as the difference between the peak and the residual shear stress or, in the experiments, the steady-state shear stress) at least in some fault patches[30]. In fact, the thermal weakening distance, D_{th}, decreases with increasing normal stress (Fig. 2): at typical crustal stresses (>20 MPa), $D_{th}<1$ m, which is below the typical displacement for moderate to large earthquakes. Moreover, our experimental estimate of the breakdown work, W_b, is consistent with the seismological observations. The breakdown work, which is one of the most robust earthquake source parameters retrieved from seismological data[13], is the seismological equivalent of the fracture energy[14], or the energy spent per unit fault area for the advancement of rupture. Following refs 13, 14, we define W_b as the mechanical dissipation associated with the breakdown stress drop. In the case of an exponential decay, for $\delta \gg D_{th}$

$$W_b=\int_0^{\delta}(\tau_p-\tau_{ss})\exp\left(-\frac{\delta'}{D_{th}}\right)\mathrm{d}\delta'\approx\sigma_n(\mu_p-\mu_{ss})D_{th} \quad (3)$$

the integral of the experimental shear stress curves. Equation (3) yields W_b values ranging between 1 and 42 MJ m^{-2} for most of the activated weakening mechanisms (Supplementary Information, section 4). These values are in the range of seismological W_b estimates[13,14] for moderate to large earthquakes (1 MJ m$^{-2}<W_b<$ 100 MJ m^{-2}). But earthquakes occur under higher normal stress than in these experiments; because $D_{th}=a\sigma_n^{-b}$ (with $1.13<b<1.24$; Fig. 2), from equation (3) we find that $W_b\approx(\mu_p-\mu_{ss})a\sigma_n^{-0.18}$. As a consequence, we expect a decrease in the breakdown work of 30–35% for an increase in σ_n from 20 to 200 MPa (that is, extrapolation of experimental data to natural conditions). Because field[31] and theoretical[13] investigations suggest that W_b is mostly converted to heat, the comparison between natural and experimental W_b values indicates that the individual processes governing dynamic fault weakening on experimental faults are similar to those governing natural faults. This is confirmed by the presence, in natural seismogenic faults, of fault products (solidified melts[4,22], reaction products[21], fluidized gouges[9] and so on) similar to those produced in the experiments[4,7–9,32].

We conclude that the experimental work performed using high-velocity friction apparatus indicates that faults are lubricated when they are deformed at slip rates typical of earthquakes, independent of the rock and weakening mechanism involved. Because experiments have been performed at normal stresses (<25 MPa) lower than those expected in the Earth's crust, some extrapolation is required to apply these results to seismogenic faults. A more direct verification may become available when new apparatus is developed that can perform experiments under the normal stresses expected in the crust (>50 MPa).

METHODS SUMMARY

The unpublished experiments cited in Figs 1–4 by De Paola *et al.*, Di Toro and Hirose, Mizoguchi and Hirose, and Ferri *et al.* were performed in the rotary shear apparatus in Kyoto University (now at the Kochi Institute for Core Sample Research, JAMSTEC, Japan). Experiments were conducted at room humidity with 0.1 m s$^{-1}<V<$ 1.3 m s^{-1} and $\delta>2$ m on solid cylinders (25 mm in diameter) or hollow cylinders (15/25 mm in internal/external diameter) in the case of cohesive rock and on 1-mm-thick gouge layers sandwiched between two solid rock cylinders and confined by Teflon rings[9] in the case of non-cohesive rocks. In experiments performed on non-cohesive rocks, the normal stress was in the range 0.6 MPa $<\sigma_n<$ 2 MPa, given the low tensile strength of Teflon. For cohesive rocks, the normal stress was in the range 5 MPa $<\sigma_n<$ 20 MPa. The reliability of the experimental procedure and the quality of the unpublished and published experiments reported in this study are indicated by the observations that (1) the same rock had similar frictional behaviour in different rotary shear apparatuses (and also in the torsional Kolsky bar[33], not discussed here; Supplementary Information, section 1); (2) different materials, such as metals, had different mechanical behaviour under similar experimental conditions (Supplementary Information, section 1); and (3) one data set (for novaculite[3]) covers the whole slip-rate interval (from 1 μm s^{-1} to 0.1 m s^{-1}) and the transition from high friction values (with results compatible with those obtained in conventional biaxial and triaxial apparatuses in the overlapping low-slip-rate range).

Full Methods and any associated references are available in the online version of the paper at www.nature.com/nature.

Received 29 January 2010; accepted 17 January 2011.

1. Scholz, C. H. *The Mechanics of Earthquakes and Faulting* (Cambridge Univ. Press, 2002).
2. Goldsby, D. L. & Tullis, T. E. Low frictional strength of quartz rocks at subseismic slip rates. *Geophys. Res. Lett.* **29,** 1844 (2002).
3. Di Toro, G., Goldsby, D. L. & Tullis, T. E. Friction falls towards zero in quartz rock as slip velocity approaches seismic rates. *Nature* **427,** 436–439 (2004).
4. Di Toro, G. & Hirose, T. Nielsen, S. Pennacchioni, G. & Shimamoto, T. Natural and experimental evidence of melt lubrication of faults during earthquakes. *Science* **311,** 647–649 (2006).

5. Hirose, T. & Shimamoto, T. Growth of molten zone as a mechanism of slip weakening of simulated faults in gabbro during frictional melting. *J. Geophys. Res.* **110,** B05202 (2005).
6. Nielsen, S., Di Toro, G., Hirose, T. & Shimamoto, T. Frictional melt and seismic slip. *J. Geophys. Res.* **113,** B01308 (2008).
7. Han, R., Shimamoto, T., Hirose, T., Ree, J.-H. & Ando, J. Ultralow friction of carbonate faults caused by thermal decomposition. *Science* **316,** 878–881 (2007).
8. Han, R., Hirose, T. & Shimamoto, T. Strong velocity weakening and powder lubrication of simulated carbonate faults at seismic slip rates. *J. Geophys. Res.* **115,** B03412 (2010).
9. Mizoguchi, K., Hirose, T., Shimamoto, T. & Fukuyama, E. High-velocity frictional behavior and microstructure evolution of fault gouge obtained from Nojima fault, southwest Japan. *Tectonophysics* **471,** 285–296 (2009).
10. De Paola, N. *et al.* Fault lubrication and earthquake propagation in thermally unstable rocks. *Geology* **39,** 35–38 (2011).
11. Fox, P. G. Mechanically initiated chemical reactions in solids. *J. Mater. Sci.* **10,** 340–360 (1975).
12. Fisher, T. E. Tribochemistry. *Annu. Rev. Mater. Sci.* **18,** 303–323 (1988).
13. Cocco, M. & Tinti, E. Scale dependence in the dynamics of earthquake propagation: evidence from seismological and geological observations. *Earth Planet. Sci. Lett.* **273,** 123–131 (2008).
14. Rice, J. R. Heating and weakening of faults during earthquake slip. *J. Geophys. Res.* **111,** B05311 (2006).
15. Byerlee, J. D. Friction of rocks. *Pure Appl. Geophys.* **116,** 615–626 (1978).
16. Brace, W. F. & Byerlee, J. D. Stick slip as a mechanism for earthquakes. *Science* **168,** 990–992 (1966).
17. Scholz, C. H. Earthquakes and friction laws. *Nature* **391,** 37–42 (1998).
18. Marone, C. Laboratory-derived friction laws and their application to seismic faulting. *Annu. Rev. Earth Planet. Sci.* **26,** 643–696 (1998).
19. Dieterich, J. H. Modeling of rock friction 1. Experimental results and constitutive equations. *J. Geophys. Res.* **84,** 2161–2168 (1979).
20. Heaton, T. H. Evidence for and implications of self healing pulses of slip in earthquake rupture. *Phys. Earth Planet. Inter.* **64,** 1–20 (1990).
21. Hirono, T. *et al.* A chemical kinetic approach to estimate dynamic shear stress during the 1999 Taiwan Chi-Chi earthquake. *Geophys. Res. Lett.* **34,** L19308 (2007).
22. Sibson, R. H. Generation of pseudotachylyte by ancient seismic faulting. *Geophys. J. R. Astron. Soc.* **43,** 775–794 (1975).
23. Di Toro, G., Hirose, T., Nielsen, S. & Shimamoto, T. in *Radiated Energy and the Physics of Faulting* (eds Abercrombie, R., McGarr, A., Di Toro, G. & Kanamori, H.) 121–134 (Geophys. Monogr. Ser. 170, American Geophysical Union, 2006).
24. Heinicke, G. *Tribochemistry* (Carl-Hanser, 1984).
25. Hsu, S. M., Zhang, J. & Yin, Z. The nature and origin of tribochemistry. *Tribol. Lett.* **13,** 131–139 (2002).
26. Steinike, U. & Tkáčová, K. Mechanochemistry of solids—real structure and reactivity. *J. Mater. Synth. Process.* **8,** 197–203 (2000).
27. Baláž, P. *Mechanochemistry in Nanoscience and Minerals Engineering* (Springer, 2008).
28. Beeler, N. M., Tullis, T. E. & Goldsby, D. L. Constitutive relationships and physical basis of fault strength due to flash heating. *J. Geophys. Res.* **113,** B01401 (2008).
29. Reches, Z. & Lockner, D. A. Fault weakening and earthquake instability by powder lubrication. *Nature* **467,** 452–455 (2010).
30. Noda, H., Dunham, E. M. & Rice, J. R. Earthquake ruptures with thermal weakening and the operation of major faults at low overall stress levels. *J. Geophys. Res.* **114,** B07302 (2009).
31. Ma, K. F. *et al.* Slip zone and energetics of a large earthquake from the Taiwan Chelungpu-fault Drilling Project (TCDP). *Nature* **444,** 473–476 (2006).
32. Brantut, N., Schubnel, A., Rouzaud, J.-N., Brunet, F. & Shimamoto, T. High-velocity frictional properties of a clay bearing fault gouge and implications for earthquake mechanics. *J. Geophys. Res.* **113,** B10401 (2008).
33. Yuan, F. & Prakash, V. Use of a modified torsional Kolsky bar to study frictional slip resistance in rock-analog materials at coseismic slip rates. *Int. J. Solids Struct.* **45,** 4247–4263 (2008).

Supplementary Information is linked to the online version of the paper at www.nature.com/nature.

Acknowledgements G.D.T. thanks T. Tullis and D. Goldsby for introducing him to this topic. G.D.T. was supported by a Progetti di Eccellenza Fondazione Cassa di Risparmio di Padova e Rovigo and by European Research Council Starting Grant Project 205175.

Author Contributions G.D.T. wrote the paper. S.N. wrote the Methods. Original and unpublished experimental work reported in the paper: N.D.P., R.H., F.F., G.D.T., T.H. and K.M. Concept development: G.D.T., R.H., S.N., M.C., N.D.P., T.H. and T.S.

Author Information Reprints and permissions information is available at www.nature.com/reprints. The authors declare no competing financial interests. Readers are welcome to comment on the online version of this article at www.nature.com/nature. Correspondence and requests for materials should be addressed to G.D.T. (giulio.ditoro@unipd.it).

METHODS

Estimate of the temperature in the slipping zone during the transient. The general solution for temperature, $T(t)$, in a semi-infinite solid given a time-varying heat flow function, $\Phi(t)$, imposed at the boundary of the solid ($z = 0$) is[34]

$$T(t) = \frac{1}{2\rho c_p \sqrt{\pi\kappa}} \int_0^t \frac{\Phi(t-\xi)}{\sqrt{\xi}} e^{-z^2/4\kappa\xi} \, d\xi \quad (4)$$

where the factor of two in the denominator of the prefactor accounts for bilateral heat diffusion in the wall rocks, ρ is the rock density, c_p is the specific heat capacity and κ is the thermal diffusivity. The experiments were performed for a constant slip rate ($V(t) = V$) and a variable shear stress, $\tau(t)$. As a consequence, the heat flow is

$$\Phi(t) = \tau(t)V \quad (5)$$

The shear stress evolution with slip, x, during the transient of length D_{th} is approximated by an exponential decay in the form

$$\tau(x) = \tau_{ss} + (\tau_p - \tau_{ss})e^{-x/D_{th}} \quad (6)$$

where τ_{ss} and τ_p are the steady-state and peak shear stresses, respectively. Hence, for $x = D_{th}$, the thermally activated slip weakening distance over which a significant decrease in shear stress occurs, $\tau = \tau_{ss} + (\tau_p - \tau_{ss})/e$ (Fig. 1). We remark that D_{th} corresponds to one-third of the slip weakening distance proposed in ref. 35, where a slip weakening distance d_c is introduced as the displacement at which $\tau_p - \tau_{ss}$ decreases to 5% of its initial value. We consider D_{th} instead of d_c because at D_{th} the shear stress weakening (that is, the lubrication of the slipping zone) is already significant ($\tau_p - \tau_{ss}$ has decreased to 36.8%, or 1/e, of its initial value), indicating that the responsible chemical reactions or phase changes have been already triggered. Moreover, the mathematical description using 1/e is simpler. By replacing x with t in equation (6) and using $x = Vt$, we obtain

$$\tau(t) = \tau_{ss} + (\tau_p - \tau_{ss})e^{-Vt/D_{th}}$$

and equation (5) results in

$$\Phi(t) = \left[\tau_{ss} + (\tau_p - \tau_{ss})e^{-Vt/D_{th}}\right]V \quad (7)$$

From equation (7), equation (4) is

$$T(t) = \frac{1}{2\rho c_p \sqrt{\pi\kappa}} \int_0^t \frac{\left[\tau_{ss} + (\tau_p - \tau_{ss})e^{-V(t-\xi)/D_{th}}\right]V e^{-z^2/4\kappa\xi}}{\sqrt{\xi}} \, d\xi \quad (8)$$

On solving the integral and considering the temperature at the boundary $z = 0$, we obtain the temperature at time t:

$$T(t) = \frac{V\left[2\tau_{ss}\sqrt{t} + (\tau_p - \tau_{ss})e^{-Vt/D_{th}}\sqrt{\pi D_{th}/V}\,\mathrm{Erfi}\left(\sqrt{Vt/D_{th}}\right)\right]}{2\rho c_p \sqrt{\pi\kappa}} \quad (9)$$

To determine the temperature at $z = 0$ (border of the slipping zone) after a slip D_{th} has occurred, we may use equation (9) to show that

$$T(t = D_{th}/V) = \frac{\sqrt{D_{th}V}\left[2e\tau_{ss} + (\tau_p - \tau_{ss})\sqrt{\pi}\,\mathrm{Erfi}(1)\right]}{2e\rho c_p \sqrt{\pi\kappa}} \quad (10)$$

where $e = 2.7182$ and $\mathrm{Erfi}(1) = 1.65043$. The temperature estimated from equation (10) has to be added to the initial (ambient) temperature to determine the actual temperature in the slipping zone. Equation (10) should overestimate the temperature increase after a slip distance D_{th}, as it does not include the heat losses by radiation from the sample, interaction of the heated slipping zone with air (the air cools the sample as the sample rotates up to 1,500 r.p.m.), expulsion of hot material from the slipping zone (for experiments performed in cohesive rocks) or heat exchange due to the tribochemical reactions triggered during frictional sliding (for example, the enthalpy energy of decarbonation of calcite is about 1.8 MJ kg^{-1}). However, the samples used in the experiments are cylinders or rings of rock. It follows that the determination of slip rate, V, in equation (10) is not straightforward, as V increases with sample radius, r ($V = \omega r$, where ω is the rotary speed). The slip rate in the slipping zone is obtained in terms of 'equivalent slip rate' V_e (refs 5, 36):

$$V_e = \frac{4\pi R r}{3}$$

where R is the revolution rate of the motor. We refer to the equivalent slip rate simply as slip rate in our study. As a consequence, equation (10) estimates the average temperature in the slipping zone, as it is calculated from the equivalent slip rate, V_e, and, for instance, the actual temperatures achieved at the sample edge might be slightly higher than those predicted from equation (10). This might explain the small underestimation of temperature predicted with equation (10) with respect to the temperatures measured at particular points of the sample during the experiments[8]. Lastly, the estimate from equation (10) of the temperature increase in the slipping zone implies the determination of thermal parameters (for example thermal diffusivity) that vary with temperature and with rock texture. We conclude that equation (10) yields a rough but useful, at least for the purposes of this study, estimate of the temperature increase in the slipping zone.

Equivalent shear stress during the transient stage. The equivalent shear stress, τ_e, is a constant shear stress that would yield the same temperature at the boundary $z = 0$ at time $t_{th} = D_{th}/V$ as the approximate exponential decay observed in the experiments (Fig. 1). As a consequence, to determine τ_e we equated the temperature achieved under constant τ_e to the temperature under the exponential decay (equation (8)):

$$\frac{1}{2\rho c_p \sqrt{\pi\kappa}} \int_0^t \frac{\tau_e V}{\sqrt{\xi}} \, d\xi = \frac{1}{2\rho c_p \sqrt{\pi\kappa}} \int_0^t \frac{\left[\tau_{ss} + (\tau_p - \tau_{ss})e^{-V(t-\xi)/D_{th}}\right]V}{\sqrt{\xi}} \, d\xi$$

By simplifying and extracting τ_e, we find that

$$\tau_e = \frac{\int_0^t \left(\left[\tau_{ss} + (\tau_p - \tau_{ss})e^{-V(t-\xi)/D_{th}}\right]/\sqrt{\xi}\right) d\xi}{\int_0^t \left(1/\sqrt{\xi}\right) d\xi}$$

Upon integration we obtain

$$\tau_e = \tau_{ss} + \frac{\sqrt{\pi}\,\mathrm{Erfi}(1)}{2e}(\tau_p - \tau_{ss}) \quad (11)$$

with $e = 2.7182$ and $\mathrm{Erfi}(1) = 1.65043$. We used equation (11) in the power density plots reported in the main text (Fig. 4).

Plot of the reaction-speed-constant curves in the friction versus power density. In Fig. 4b, c, we plotted the reaction speed constant curves versus power density, $\tau_e V$.

By combining equations (10) and (11), we find that the temperature increase in the slipping zone after a slip distance D_{th} is

$$\Delta T(t = D_{th}/V) = \frac{\tau_e V}{\rho c_p \sqrt{\pi\kappa}} \sqrt{\frac{D_{th}}{V}}$$

As a consequence, the reaction speed constant is

$$k = A\exp\left(\frac{-E_A}{R(T_{amb} + \Delta T)}\right) = A\exp\left(\frac{-E_A}{R\left(T_{amb} + (\tau_e V/\rho c_p)\sqrt{D_{th}/\pi\kappa V}\right)}\right) \quad (12)$$

where T_{amb} is the room temperature. Equation (12) allows us to determine the reaction speed constant for a given power density once D_{th} is known. Figure 4 includes experiments performed over a broad range of normal stresses and slip rates. As reported in Fig. 2, for a given rock D_{th} decreases with increasing normal stress and, for a given power density, $\tau_e V$, the reaction speed constant varies with $\sqrt{D_{th}/V}$ (equation (12)). We therefore considered the smallest and largest $\sqrt{D_{th}/V}$ values for a given rock type, resulting in the two reaction-speed-constant curves (for the same reaction) reported in Fig. 4b, c. The thermal properties (ρ, c_p and κ) of the different rocks (Supplementary Information, section 5) at a temperature of 300 K were considered in equation (12) and in Fig. 4b, c.

34. Carslaw, H. S. & Jaeger, J. C. *Conduction of Heat in Solids* 2nd edn, 76 (Clarendon, 1959).
35. Mizoguchi, K., Hirose, T., Shimamoto, T. & Fukuyama, E. Reconstruction of seismic faulting by high-velocity friction experiments: an example of the 1995 Kobe earthquake. *Geophys. Res. Lett.* **34,** L01308 (2007).
36. Shimamoto, T. & Tsutsumi, A. A new rotary-shear high-speed frictional testing machine: its basic design and scope of research [in Japanese with English abstract]. *J. Tecton. Res. Group Jpn* **39,** 65–78 (1994).